

Full Length Research Paper

Effect of temperature treatment on the optical characterization of ZnO-Bi₂O₃-TiO₂ varistor ceramics

M. G. M. Sabri¹, B. Z. Azmi^{1,2*}, Zahid Rizwan³, M. K. Halimah¹, M. Hashim¹ and M. H. M. Zaid¹

¹Department of Physics, Faculty of Science, Universiti Putra Malaysia, 43400 UPM Serdang, Selangor, Malaysia.

²Advanced Materials and Nanotechnology Laboratory, Institute of Advanced Technology, Universiti Putra Malaysia, 43400 UPM Serdang, Selangor, Malaysia.

³National Textile University, Sheikhpura Road, Faisalabad (37610), Pakistan.

Accepted 21 February, 2011

The optical band-gap energy (E_g) is an important feature of semiconductors which determines their applications in optoelectronics. So, it is necessary to investigate the electronic states of ceramic ZnO and effect of doped impurities at different processing conditions. E_g of the ceramic ZnO + xBi₂O₃ + xTiO₂ where x = 0.5 mol%, was determined using UV-Vis spectrophotometer. The samples were prepared using solid-state route and sintered at the sintering temperatures from 1140 to 1260°C for 45 min in open air. E_g was decreased with increase of sintering temperature. XRD analysis indicates that there is hexagonal ZnO and few small peaks of inter granular layers of secondary phases, namely, Bi₄Ti₃O₁₂ and Zn₂Ti₃O₈. The relative density of the sintered ceramics decreased and the average grain size increased with the increase of sintering temperature. The variation of sintering temperatures and XRD findings are correlated with the UV-Vis spectrophotometer results of ZnO doped with 0.5 mol% of Bi₂O₃ and TiO₂ due to the formation of interface states at all sintering temperatures.

Key words: Optical band-gap, ZnO, Bi₂O₃, TiO₂.

INTRODUCTION

Polycrystalline Zinc Oxide (ZnO) is used extensively in rubber, paint, cosmetics and textile industries as well as in electronic industry (Ammar and Farag, 2010; Clarke, 1999; Feng et al., 2010; Look, 2001). The ZnO based varistor is widely used as an electronic component in automobile electronics and also in sophisticated semiconductor electronic. ZnO based varistor is fabricated with different types of additives which play important roles in its non-linear characteristics. Its unique grain boundary feature is responsible for non-linear current-voltage (*I-V*)

characteristics of the device (Clarke, 1999; Souza et al., 2003) and thus, is used to protect electrical equipment against unwanted electrical surges. Currently, ZnO based varistors are being used for low-voltage applications. ZnO based varistor is fabricated with different metal oxides of small amounts such as Bi₂O₃, CoO, MnO, Sb₂O₃, and TiO₂ (Matsuoka, 1971; Snow et al., 1980; Eda, 1989; Bai et al., 1995; Toplan et al., 1997; Fah and wang, 2000). *I-V* studies have been extensively investigated for the ZnO based varistor by previous researchers (Eda, 1989; Choon and Byoung, 2003) and it is necessary to investigate the electronic states of ceramic ZnO and the effect of doped impurities at different processing conditions. The measurement of the absorption spectrum in semiconductors leads to the determination of the optical band-gap energy (Ghoosh et al., 1995; Zelaya et al., 1994).

In this study, the investigation regarding the optical properties and relationship with X-ray Diffraction (XRD) findings of ZnO doped with Bi₂O₃ and TiO₂ at different

*Corresponding author. E-mail: azmizak@gmail.com. Tel: (603)89466650. Fax: (603)89454454.

Abbreviations: ZnO, Zinc oxide; XRD, X-ray diffraction; FWHM, Full width of half maximum; VPSEM, Variable Pressure Scanning Electron Microscopy.

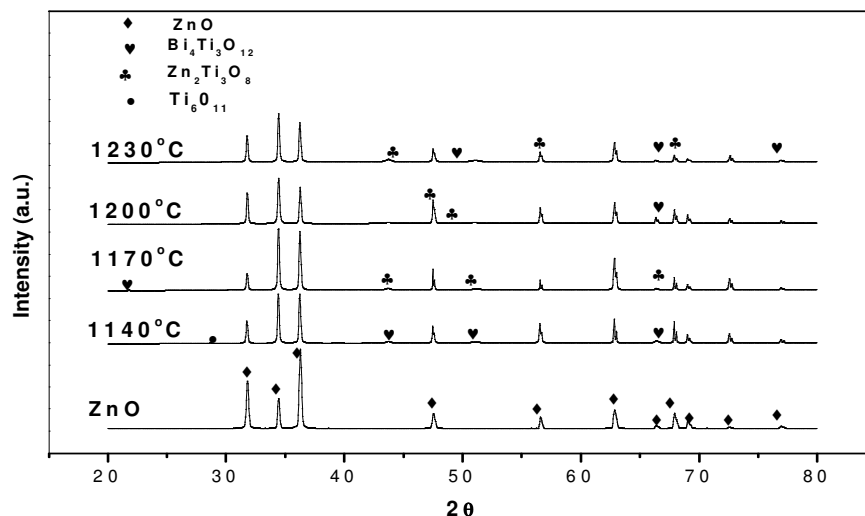


Figure 1. XRD patterns of ZnO based ceramic varistor at different sintering temperatures.

sintering temperatures are discussed.

EXPERIMENTAL PROCEDURE

Oxide precursors of 99.9% purity (Alfa Aesar) were used. The composition consists of 99 mol% ZnO + 0.5 mol% Bi₂O₃ + 0.5 mol% TiO₂ powder. The powder was ball milled for 24 h in deionised water. The slurry was dried at 70°C using hot plate and continuously magnetically stirred to avoid the sedimentation of the heavy particle and pre-sintered at 800°C for two hours in open air with heating and cooling rate of 6°C min⁻¹. The pre-sintered mixture was pulverized using an agate mortar/pestle and after 1.75 wt.% Polyvinyl Alcohol binder addition, granulated by sieving 75 micron mesh screen. The mixture was then pressed into discs of 10 mm in diameter and 1 mm in thickness, each at a pressure of 2 ton/m². Finally, the discs were sintered at 1140, 1170, 1200, 1230 and 1260°C in open air for 45 min sintering duration at heating and cooling rate of 2.66°C min⁻¹. The disk from each sample was ground for optical and XRD characterizations.

The crystalline phases were identified by an XRD (PANalytical X'Pert Pro PW3040/60, Philips) with CuK α radiation and the data were analyzed, using X'Pert High Score software. The density was measured by the geometrical method taking the average of 10 disks (Wang et al., 2005). For the microstructure analysis, each of the disk samples was thermally etched at 150 °C in a tube furnace.

The microstructure was examined by Variable Pressure Scanning Electron Microscopy (VPSEM, Leo 1455). The average grain size (d) was determined by lineal intercept method (Wurst and Nelson, 1972), given by:

$$d = 1.56L/MN \quad (1)$$

where L is the random line length on the micrograph, M is the magnification of the micrograph and N is the number of the grain boundaries intercepted by lines.

The UV-Vis spectrophotometer was used to measure the optical band-gap energy of the ceramics. The transmission signal was measured for the wavelength from 200 to 800 nm and then

converted to absorption signal for further evaluation (Gonzalez et al., 2002). It was assumed that the fundamental absorption edge of the ceramics is due to the direct allowed transition. The optical band-gap energy is given by the expression (Smith, 1978):

$$(Ahu)^2 = C(hu - E_g) \quad (2)$$

where A is the optical absorption coefficient, C is the constant independent of photon energy (hu), and E_g is the direct allowed optical band-gap energy. From the plot of $(Ahu)^2$ versus hu , the value of E_g is obtained by using Origin Pro 8.0 software within the linear fitted regions at $(Ahu)^2=0$.

RESULTS AND DISCUSSION

The XRD analysis (Figure 1), reveals diffraction peaks which belong to two phases, that is, ZnO (ICSD code: 067454) and inter granular layers in the varistor ceramics. The inter granular layers are composed of Ti₆O₁₁ (ref. code: 00-018-1401) and appeared as a very small peak in the XRD pattern for the sample sintered at 1140°C for 45 min sintering time only. Many secondary phases with small peaks were detected in the ceramics, namely, Bi₄Ti₃O₁₂ (ICSD code: 024735) and Zn₂Ti₃O₈ (ICSD code: 022381) at all sintering temperatures. Figure 2a shows the dependence of the full width of half maximum (FWHM) of the XRD peaks for the plane (100) of ZnO on the sintering temperature. The FWHM for ZnO at plane (100) slightly decreases with the increase of sintering temperature which indicates a structural ordering of ZnO inside the grain and grain boundaries. However, the FWHM of Bi₄Ti₃O₁₂ (640 plane), (Figure 2b), increases with the increase of sintering temperature, which indicates a structural disordering of impurities at the grain boundaries in ZnO ceramic. The results agree

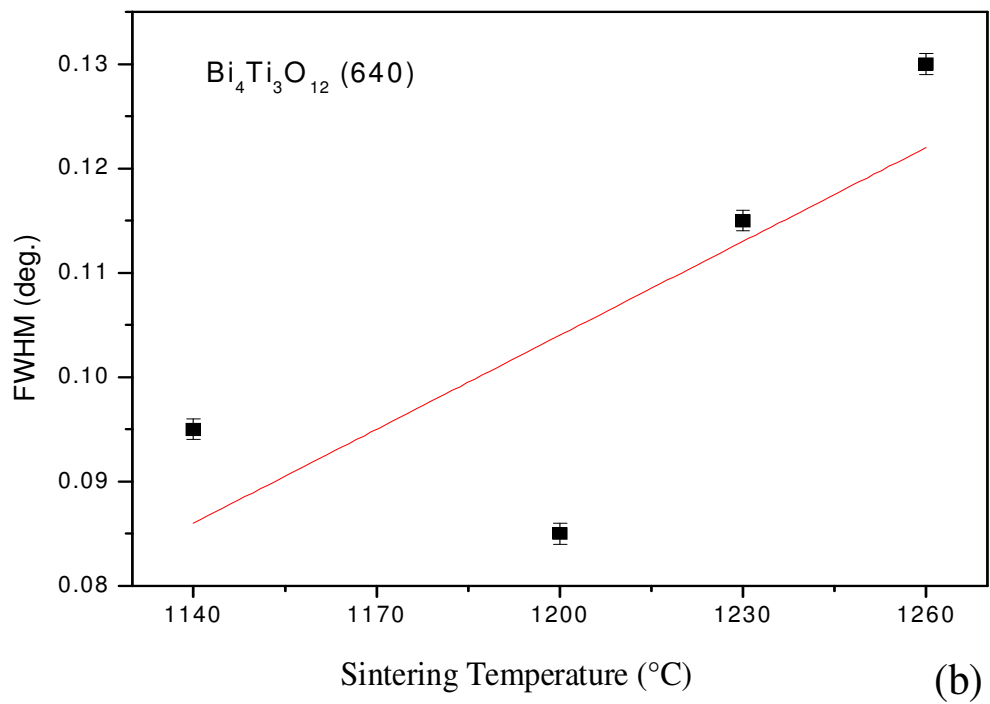
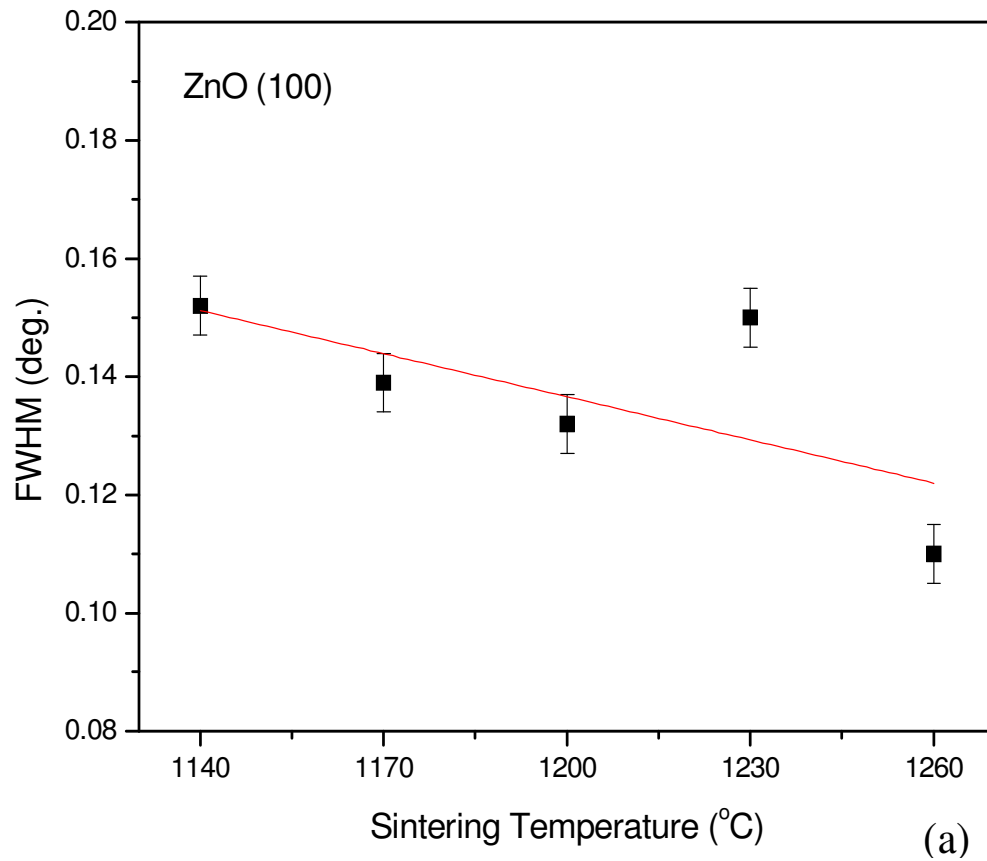


Figure 2. Dependence of the FWHM of XRD peaks at (a) (100 plane for ZnO) and (b) (640 plane for $\text{Bi}_4\text{Ti}_3\text{O}_{12}$ ceramics).

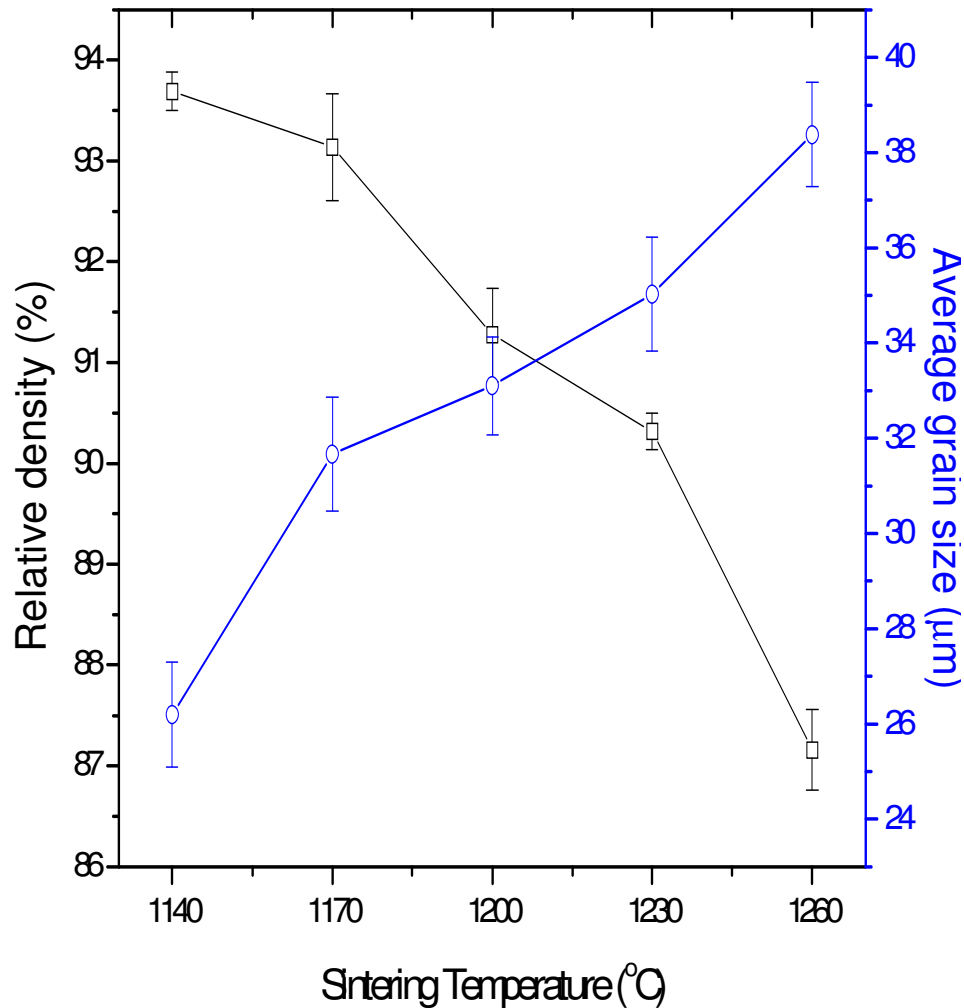


Figure 3. (a) Relative density (%) and (b) average grain size of ZnO ceramics at different sintering temperatures.

with Toyoda and Shimamoto, (1998) that dealt only with ZnO and Bi₂O₃.

The relative density of sintered ceramics decreases with the increase of sintering temperature from 93.70 to 87.16% of theoretical density (5.67 g/cm³), (Figure 3a). The average grain size increased from 26.2 to 38.4 μm with the increase of sintering temperature, (Figure 3b). This increase in average grain size is due to the TiO₂ which is a strong grain enhancer. It was observed under VPSEM that a few abnormal grains of irregular shapes and size were distributed in the whole sample especially at high sintering temperature. The abnormal grain growth increases with increase of sintering temperature, (Figure 4). This indicates that the pores increase with the increase of sintering temperature. The pores are trapped between the large grains in the ceramics at high sintering temperature (Sabri et al., 2009).

E_g is estimated from the plot of $(Ahu)^2$ against hu , (Figure 5), and are 2.96 eV at the sintering temperature 1140°C, 2.99 eV at 1170°C, 2.97 eV at 1200°C, 2.92 eV at 1230°C and 2.94 eV at 1260°C, (Figure 6). E_g is decreased compared to the pure ZnO (3.2 eV). It is observed through linear fitting of the data that the trend in E_g is decreasing. The liquid phase of Bi₂O₃ generates the interface state which reduces the E_g of pure ZnO (Toyoda and Shimamoto, 1998). Doping TiO₂ in ZnO-Bi₂O₃ system slightly reduces the E_g . Only 1140°C sintering temperature shows that the limited substitution of Ti⁴⁺ ions in the ZnO lattice as the ionic radii of Ti⁴⁺ (0.68 Å) is smaller than that of Zn²⁺ (0.74 Å) as evidence in XRD findings, Figure 1. The addition interface states are generated that reduces the E_g at other higher temperatures. This reduction of E_g correlates with the structural disordering increment of Bi₄Ti₃O₁₂ in the grain boundaries with the

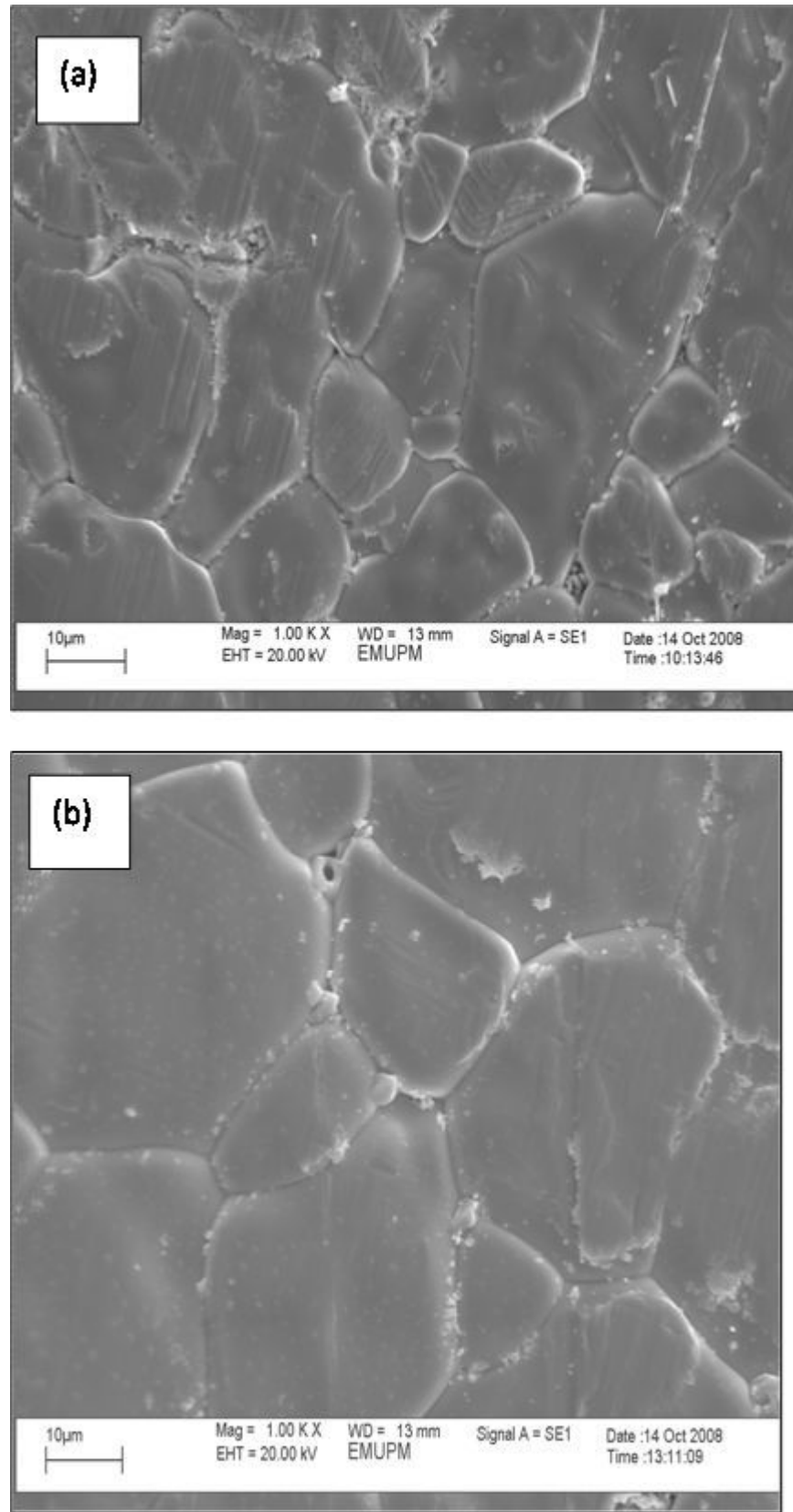


Figure 4. SEM micrographs of ceramics after sintering at (a) 1170°C and (b) 1260°C.

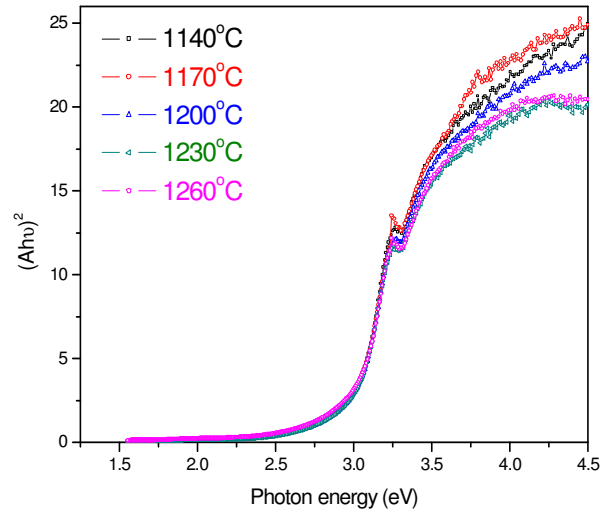


Figure 5. Optical absorption spectra of ZnO ceramics at different sintering temperatures.

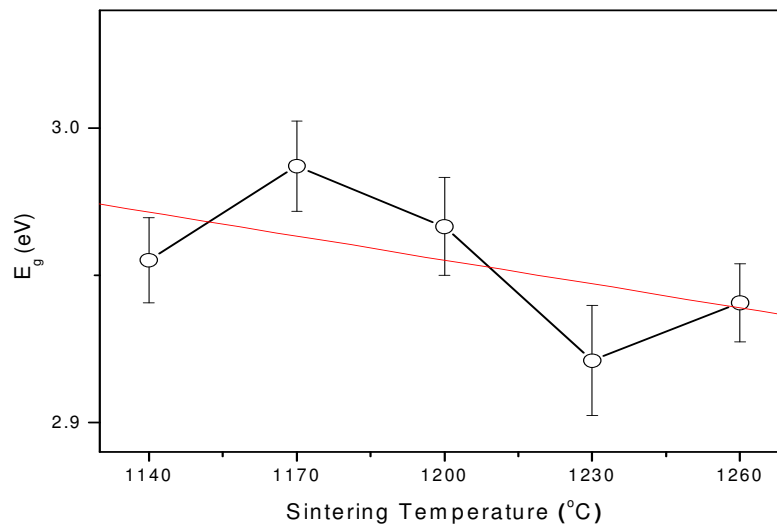


Figure 6. The variation of optical band-gap energy with sintering temperatures.

increase of sintering temperature.

structural disordering in the grain boundaries.

Conclusions

The ZnO ceramics Optical band gap energy decreases with the increase of sintering temperature. It shows the segregation Bi_2O_3 at grain boundaries and possibly substitution of Ti ion with Zn ion which creates interface states within the forbidden region. These results are correlated with the analysis obtained by XRD which shows a

ACKNOWLEDGEMENTS

The authors gratefully acknowledge the financial support for this work from Ministry of Higher Education of Malaysia under Research University Grant Scheme (RUGS) of Project No. 05-01-09-0754RU. One of the author's is grateful to Department of Physical Sciences, Faculty of Science and Technology, Universiti Malaysia

Terengganu and Ministry of Higher Education for supporting the studies.

REFERENCES

- Ammar AH, Farag AAM (2010). Investigation of deep level transient spectroscopy (DLTS) of dopant ZnO-based varistors, *Phys. B.*, 405:1518.
- Bai SN, Shieh JS, Tseng Ty (1995). Characteristic analysis of ZnO varistors made with spherical precipitation powders, *Mater. Chem. Phys.*, 41:104-109.
- Choon WN, Byoung-Chil S (2003). Highly stable nonlinear properties of ZnO-Pr₆O₁₁-CoO-Cr₂O₃-Y₂O₃-based varistor ceramics. *Mater. Lett.*, 57:1322-1326.
- Clarke DR (1999). Varistor ceramics. *J. Am. Ceram. Soc.*, 82(3):485-502.
- Eda K (1989). Zinc oxide varistor. *IEEE Elect. Insul. Mag.*, 5: 28-41.
- Fah CP, Wang J (2000). Effect of high-energy mechanical activation on the microstructure and electrical properties of ZnO-based varistors. *Solid State Ionics*. 132:107-117.
- Feng H, Peng Z, Fu X, Fu Z, Wang C, Qi L, Miao H (2010). Effect of TiO₂ doping on microstructural and electrical properties of ZnO-Pr₆O₁₁-based varistor ceramics, *J. Alloy. Compd.*, 497: 304.
- Ghoosh AK, Som KK, Chatterjee S, Chaudhuri BK (1995). Photoacoustic spectroscopic study of energy gap, optical absorption, and thermal diffusivity of polycrystalline ZnSe_xTe_{1-x} (0 <= x <= 1) alloys. *Phys. Rev. B.*, 51(8):4842-4848.
- Gonzalez-Hernandez J, Gorley PM, Holrley PP, Vartsabyuk OM, Vorobiev Yu V (2002). X-Ray, kinetic and optical properties of thin CuInS₂ films. *Thin Solid Films*. 403-404:471-475.
- Look DC (2001). Recent advances in ZnO materials and devices, *Mat. Sci. Eng. B-Solid.*, 80:383.
- Matsuoka M (1971). Non-ohmic properties of zinc oxide ceramics. *Jpn. J. Appl. Phys.*, 10 (6):736-746.
- Sabri MGM, Azmi BZ, Zahid Rizwan, Halimah MK, Hashim M and Sidek HAA (2009). Application of direct current and temperature stresses of low-voltage ZnO based varistor ceramics. *Am. J. Appl. Sci.*, 6(8): 1591-1595.
- Smith RA (1978). *Semiconductors*. 2nd ed. Cambridge University Press: Cambridge.
- Snow GS, White SS, Cooper RA, Armijo JR (1980). Characterization of high field varistors in the system ZnO-CoO-PbO-Bi₂O₃. *Am. Ceram. Soc. Bull.*, 59 (6):617-622.
- Souza FL, Gomez JW, Bueno PR, Cassia-Santos MR, Araujo AL, Leiti ER, Longo E, Varela AJ (2003). Effect of the addition of ZnO seeds on the electrical properties of ZnO-based varistors. *Mater. Chem. Phys.*, 80:512-516.
- Toplan O, Gunay V, Ozkan OT (1997). Grain growth in the MnO added ZnO-6 wt% Sb₂O₃ ceramic system. *Ceram. Int.*, 23 (5):251-255.
- Toyoda T, Shimamoto S (1998). Effect of Bi₂O₃ impurities in ceramic ZnO on photoacoustic spectra and current-voltage characteristics. *Jpn. J. Appl. Phys.*, 37:2827-2831.
- Wang JF, Wen-Bin S, Hong-Cun C, Wen-Xin W, Guo-Zhong Z (2005). (Pr, Co, Nb)-Doped SnO₂ Varistor Ceramics. *J. Am. Ceram. Soc.*, 88 (2):331-334.
- Wurst JC, Nelson JA (1972). Lineal intercept technique for measuring grain size in two-phase polycrystalline ceramics. *J. Am. Ceram. Soc.*, 55: 109-111.
- Zelaya-Angel O, Alvarado-Gil JJ, Lozada-Morales R (1994). Band-gap shift in CdS semiconductor by photoacoustic spectroscopy: Evidence of a cubic to hexagonal lattice transition. *Appl. Phys. Lett.*, 64(3): 291-293.